

# Dual-Band Planar Inverted-F Antenna with Enhanced Bandwidth by Adding a T-Shaped Slot and a Two Elements for Mobile Phone Applications

Mustapha El Halaoui\*, Abdelmoumen Kaabal,  
Hassan Asselman, Saida Ahyoud, and Adel Asselman

**Abstract**—In this article, a compact planar inverted-F antenna with a wide frequency band for WLAN, Bluetooth, HiperLAN, LTE2500, and WiMAX applications in mobile handsets is proposed. The designed PIFA provides two operating bands at 2.5 GHz with a bandwidth of 300 MHz (13%) and at 5.2 GHz with a bandwidth of 5700 MHz (76%). The dual-band performance and the improved bandwidths are realized by two techniques: the integration of a T-shaped slot in the radiating patch of the antenna and the addition of two elements in the side of the PIFA. The two operating bands of the antenna are controlled by adjusting the size of slot and the size of elements 1 and 2. The distribution of the specific absorption rate (SAR) of 1-g and 10-g in the head of human tissues for two positions of the antenna at 2.5 GHz and 5.2 GHz is also studied. The results of simulation and measurement of the proposed antenna are presented and discussed.

## 1. INTRODUCTION

During the last decade, the growing and increasing trend in demand of the use of wireless communication technologies has led to a widespread use of the frequency bands of 2.4 GHz and 5.2 GHz for the wireless local area network. This growth requires an increase of miniaturized components for mobile phones handsets [1]. However, the design of new compact antennas with small size, multi-band and wideband characteristics for mobile phones limited in an enclosed space for antennas has become a necessity [2]. Planar inverted-F antennas (PIFA) are widely used as internal antennas for mobile devices such as phones, smart phones, tablets and tablet computers because they are reasonably compact, having a low profile with good electrical performance, and compatible with RF circuits. They have omnidirectional radiation pattern and good Specific Absorption Rate (SAR) characteristics as well [3–5].

Numerous models of PIFA were studied to show their ultra wideband characteristic. Some researchers have worked on the improvement of the bandwidth of the PIFA antenna by using different techniques, such as the increase in width of the feeding plate and short-circuit plate [6, 7], adding parasitic elements [8, 9], integrating slots in the ground plane [10–12], using cut-etched ground plane [13], and integrating a V-shaped slot in a triangular isosceles radiating patch [14].

The objective of this article is to demonstrate a highly effective method to obtain a wide band by integrating a T-shaped slot in the radiating patch and by adding elements 1 and 2 to the feeding plate and short-circuit plate, respectively. Therefore, the new proposed PIFA can operate in two frequency bands 2.5 GHz and 5.2 GHz with a bandwidth of 13% and 76%, respectively. For good optimization of the antenna, the effects of different critical parameters on the reflection coefficient of the new PIFA

---

*Received 18 August 2015, Accepted 3 November 2015, Scheduled 9 November 2015*

\* Corresponding author: Mustapha El Halaoui (mustapha.halaoui@gmail.com).

The authors are with the Optics and Photonics Group, Faculty of Sciences, Abdelmalek Essadi University, P. O. Box: 2121, Tetouan, Morocco.

**Table 1.** Comparisons of the proposed PIFA to the previous PIFA.

Structure	Lower band	Upper band	antenna size (mm <sup>3</sup> )	Gain (dBi)
[15]	2.25–2.86 GHz (613 MHz)	4.81–6.21 GHz (1400 MHz)	19.8 × 19.8 × 4.5	3.8 at 2.4 GHz; 7.2 at 5 GHz
[16]	2.4–2.5 GHz (100 MHz)	4.5–6.25 GHz (1750 MHz)	32 × 19 × 8	1.4 at 2.4 GHz; 4.3 at 5.4 GHz
[17]	2.38–2.61 GHz (230 MHz)	4.6–5.77 GHz (1170 MHz)	17 × 17 × 5	—
proposed	2.39–2.69 GHz (300 MHz)	4.71–10.45 GHz (5740 MHz)	23 × 10 × 3	4 at 2.4 GHz; 7 at 5.4 GHz

are studied and discussed. Table 1 presents a detailed comparison between PIFAs' dual-band WLAN (Wireless Local Area Network) for mobile phones, in terms of antenna size, bandwidth, and average peak gains. The antenna geometry and parametric studies are presented in Section 2, while the results of the reflection coefficient, current distributions, radiation pattern and SAR distribution at different resonant frequencies are presented in Section 3.

## 2. ANTENNA CONFIGURATION

### 2.1. The Antenna Geometry

Planar inverted-F antenna is a development of the monopole antenna ( $\lambda/4$ ) and the microstrip patch antenna. PIFA in its basic configuration is composed of a planar patch placed in parallel with a ground plane, a short circuit that connects the radiating patch to the ground plane, and an antenna feeding mechanism. The fundamental mode resonant frequency for PIFA can be determined approximately by the equation:

$$f_0 = \frac{c}{4(W_p + L_p)} \quad (1)$$

where  $f_0$  is the resonance frequency at desired band;  $L_p$  and  $W_p$  are the length and the width of the radiating patch respectively;  $c$  is the speed of light.

Figure 1(b) shows the three-dimensional geometry of the proposed PIFA with detailed dimensions shown in Table 2 for WLAN (Wireless Local Area Network), Bluetooth, HiperLAN (HIGH PERFORMANCE Radio Local Area Network), LTE (Long Term Evolution) and WIMAX (Worldwide Interoperability for Microwave Access) operations. The proposed antenna is composed of five parts: a rectangular radiating patch with T-shaped slot (Fig. 1(d)) printed on an FR4 substrate (relative permittivity  $\epsilon_r = 4.4$ , loss tangent  $\tan \delta = 0.02$  and thickness  $hs = 1.6$  mm), a short circuit plate, a ground plane, two elements 1 and 2, and feeding antenna in the form of SMA connector. The two elements 1 and 2 are added to the feeding plate and the short circuit plate (Fig. 1(c)), respectively. To evaluate the effectiveness of integrated slots, curve (i) and curve (ii) in Fig. 2 show the simulated reflection coefficient without and with slot respectively. We observe that the slot forces the antenna to operate in another broadband. To improve the bandwidth, the two elements (1 and 2) were added to the front face of the antenna (Fig. 1(c)). Curve (iii) in Fig. 2 shows the reflection coefficient of the proposed antenna. A comparison of this coefficient between the base antenna and that proposed shows an enlargement of bandwidth by 40.5%.

### 2.2. Parametric Study of the Reflection Coefficient

The PIFA has the advantage to offer several degrees of liberty to make adjustments. Indeed, the variations of the parameters shown in Table 2 allow us to adjust the behavior of the proposed antenna.

**Table 2.** Detailed dimensions of the proposed PIFA.

Parameter	Dimension (mm)
$L_g$	125
$W_g$	60
$L_p$	10
$W_p$	23
$L_{pa}$	4
$W_{sh}$	3.5
$e$	3
$f_p$	2
$h_a$	3.2
$h_s$	1.57
$W_t$	21
$L_t$	7

In this section, parametric studies were performed and discussed to understand the effects of different dimensional parameters. This allowed us, thereafter, to achieve optimal size of the antenna and maintain a good impedance matching in the desired frequency bands. The parametric study is realized by the CST microwave studio software.

*2.2.1. The Influence of the T-Shaped Slot's Size*

Current applications require smaller antennas with multi-band and UWB operations. The integrated T-shaped slot in the upper radiating patch of the proposed antenna (Fig. 1(d)) plays a very important role in the dual-band and ultra-wideband operations. The effects of changing the size of the T-shaped slot on the reflection coefficient are studied and discussed in this section.

Figure 3 shows the reflection coefficient as a function of the frequency with the variation in the width ( $W_t$  in Fig. 1(d)) and the length ( $L_t$  in Fig. 1(d)) of the T-shaped slot while the other antenna parameters are kept constant. As observed, the reflection coefficient is very sensitive to the size of the T-shaped slot. However, we observe that with increasing the size of the slot, the resonant frequency 2.5 GHz shifts toward the lower frequency, and bandwidth at 5.2 GHz has widened from 1.9 GHz for

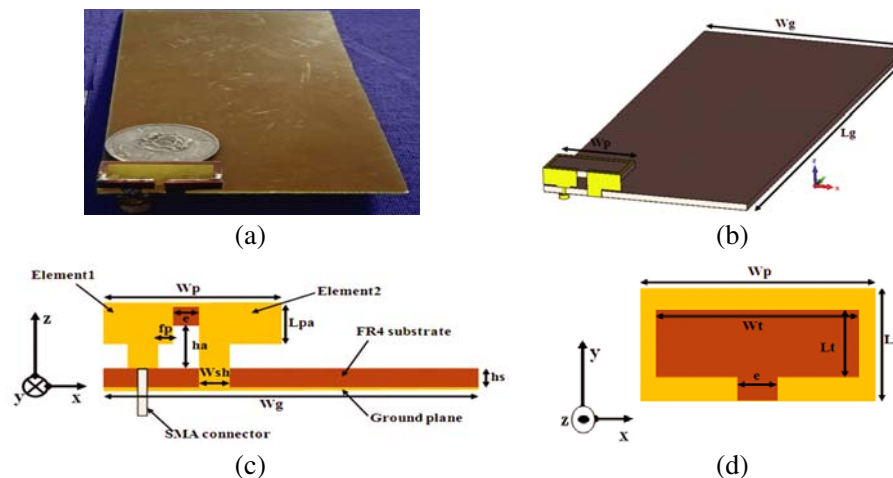


**Figure 1.** Geometry of the proposed PIFA: (a) fabricated prototype, (b) 3D view, (c) front view, and (d) top view.

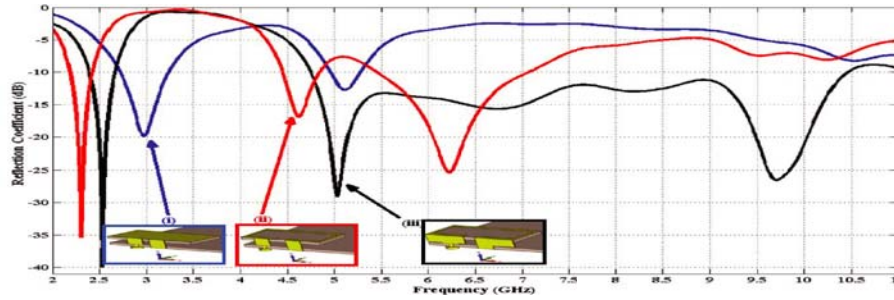


**Figure 2.** The effect of the T-shaped slot and the two elements on the reflection coefficient of the proposed PIFA.

$Wt = 18$  mm and  $Lt = 5$  mm up to  $5.7$  GHz for  $Wt = 21$  mm and  $Lt = 8$  mm.

The study of the variation of parameter  $e$  (Fig. 1(d)) is realized to characterize the effects on the reflection coefficient. Fig. 4 shows the reflection coefficient as a function of frequency for different values of parameter  $e$  ( $e = 2, 3, 4, 5$  mm), while the other antenna parameters are fixed. From this figure, we can notice that the change in parameter  $e$  does not affect the first band ( $2.5$  GHz), while the width of the 2nd band ( $5.2$  GHz) increases by increasing the value of  $e$ .

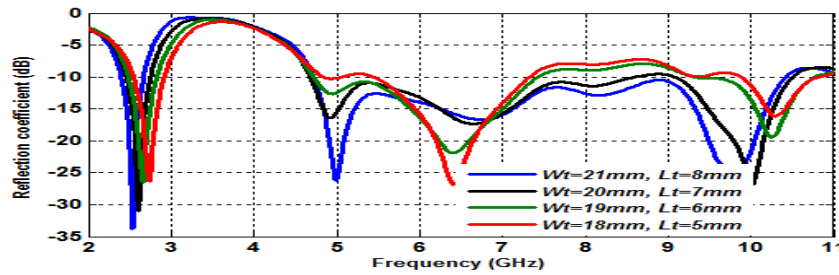


**Figure 3.** Simulated reflection coefficients with the variation of the width and the length of the T-shaped slot.

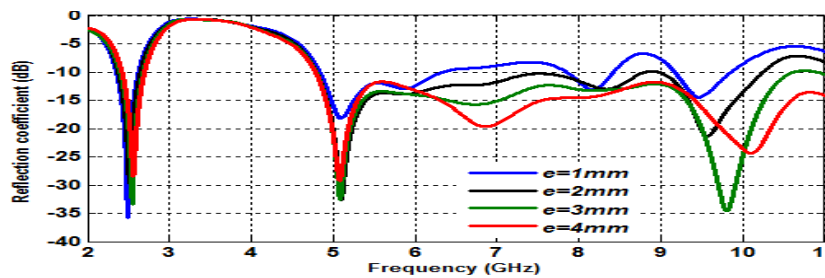


**Figure 4.** Simulated reflection coefficients with the variation of the parameter  $e$ .

### 2.2.2. The Influence of the Width of Elements 1 and 2 ( $Lpa$ in Fig. 1(c))

To analyze the behavior of elements 1 and 2 (Fig. 1(c)), a parametric study of the variation of the width of these two elements is realized in this section. Fig. 5 shows the reflection coefficient as a function of the frequency for four different values of parameter  $Lpa$  ( $Lpa = 2, 3, 4, 5$  mm). As observed, the first resonance frequency ranges from  $2.35$  GHz for  $Lpa = 2$  mm to  $2.8$  GHz for  $Lpa = 4.5$  mm, and by increasing parameter  $Lpa$ , the width of the 2nd band increases. In addition, the best bandwidth to the two modes of resonance is obtained when  $Lpa$  is bigger.

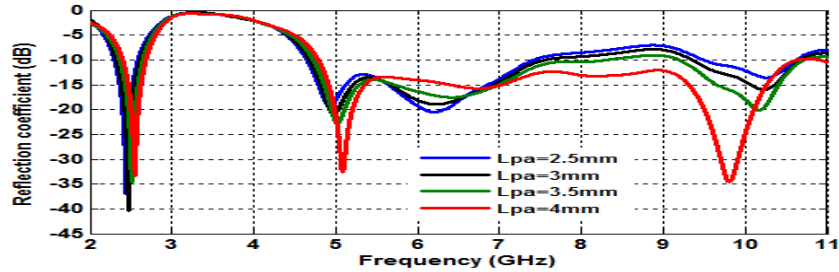


**Figure 5.** Simulated reflection coefficients with the variation of the width of the two elements.

2.2.3. The Influence of the Width of the Short-Circuit Plate ( $W_{sh}$  in Fig. 1(c))

The width of the short circuit plate strongly affects the performance of the proposed PIFA. Fig. 6 shows the effects of parameter  $W_{sh}$  on the reflection coefficient. Two observations were made:

- For the lower band (2.4–2.7 GHz), the resonance frequency increases by increasing  $W_{sh}$ .
- For the upper band (5–10 GHz), the impedance bandwidth increases by increasing  $W_{sh}$ .

So, this width also has an important impact on the upper impedance bandwidth.

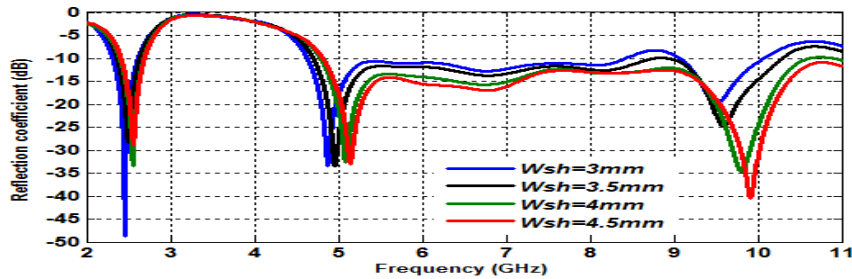


**Figure 6.** Simulated reflection coefficients with the variation of the width of the short-circuit plate.

3. ANALYSIS OF RESULTS AND DISCUSSION

3.1. The Reflection Coefficient

To validate the simulation results, the proposed antenna is fabricated on an FR-4 substrate with the same parameters in Table 2. A prototype of the fabricated antenna is shown in Fig. 1(a). Fig. 7 shows the simulated reflection coefficient by CST microwave studio and the measured reflection coefficient by the Vector Network Analyzer. This figure also shows a reasonable agreement between the results

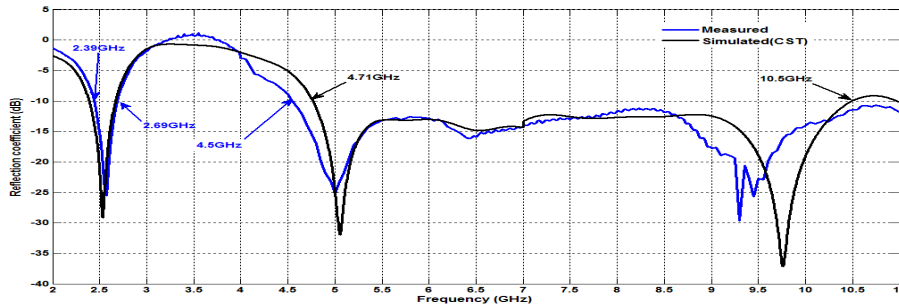


**Figure 7.** Measured and simulated reflection coefficient of the proposed PIFA.

of simulation and measurement although there is a shift in the upper frequency band justified by manufacturing errors of this small antenna. Two operating bands are obtained: the first bandwidth ( $VSWR \leq 2$ ) from 2.39 GHz to 2.69 GHz with a width of 300 MHz (13%) and the second band ultra-wide ( $VSWR \leq 2$ ) from 4.71 GHz to 10.45 GHz with a width of 5740 MHz (76%). The two bands obtained cover Wireless Local Area Network (2.4, 5.2 and 5.8 GHz), Long Term Evolution (LTE2.5 GHz), Bluetooth (2.4 GHz), Worldwide Interoperability for Microwave Access (5.5 GHz), High Performance radio Local Area Network (5.2, 5.6 GHz) bands and an additional band from 5.9 to 10.45 GHz.

### 3.2. Current Distribution

A better comprehension of the antenna behavior can be observed from surface current distribution. The current distributions at 2.5 GHz, 5.2 GHz and 9.7 GHz are shown in Fig. 8(a), Fig. 8(b) and Fig. 8(c), respectively. For 2.5 GHz frequency (Fig. 8(a)), the surface currents that circulate around the integrated slot are symmetrical and share the same electrical length. At the 5.2 GHz frequency (Fig. 8(b)), the surface currents flow on three sides of the antenna with a maximum density on the two elements, 1 and 2. For the 9.7 GHz frequency (Fig. 8(c)), the current distributions are concentrated in six parts of the antenna.

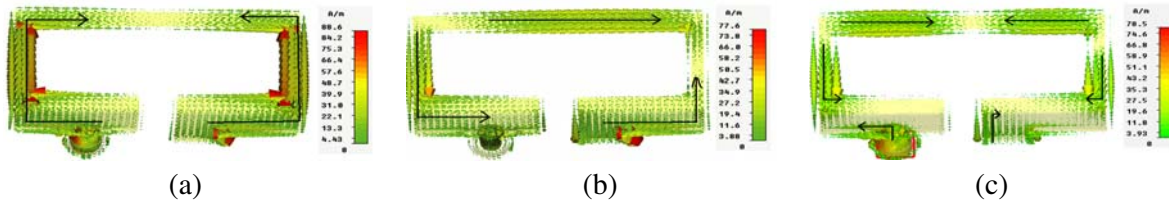


**Figure 8.** Surface current distribution of the proposed PIFA: (a) at 2.5 GHz, (b) at 5.2 GHz, and (c) 9.7 GHz.

### 3.3. Radiation Pattern and Gain

The radiation characteristics of the proposed PIFA have also been studied. Fig. 9, Fig. 10 and Fig. 11 plot the radiation patterns for the proposed PIFA at 2.5 GHz, 5.2 GHz and 9.7 GHz, respectively. The radiation patterns represent  $E_\varphi$  and  $E_\theta$  components respectively. For both frequencies, good omnidirectional radiation in the elevation plane ( $y-z$  plane) and azimuthal plane ( $x-z$  plane) is seen. The simulated gain as a function of frequency of the proposed PIFA in the broadside direction is shown in Fig. 12. A stable gain can be obtained throughout the lower band from 3.66 dBi to 4.17 dBi. The antenna gain varies from 1.5 dBi to 7.4 dBi over the upper band. The gain drops deeply to  $-8.1$  dBi from 3 GHz to 5 GHz.

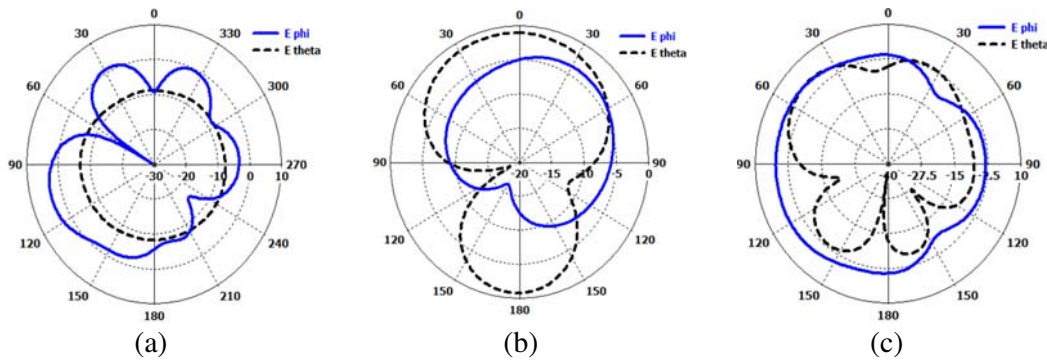


**Figure 9.** Radiation patterns of the proposed PIFA at 2.5 GHz: (a)  $x-y$  plane ( $\theta = 90$ ), (b)  $x-z$  plane ( $\varphi = 0$ ), and  $y-z$  plane ( $\varphi = 90$ ).

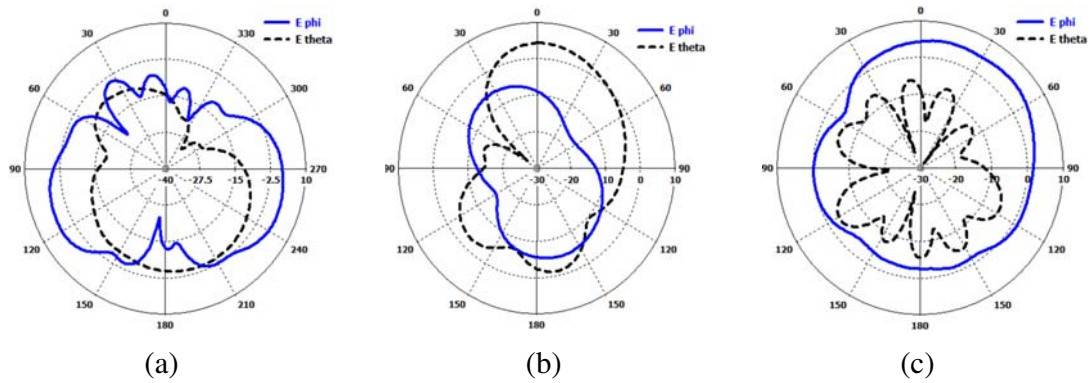


**Figure 10.** Radiation patterns of the proposed PIFA at 5.2 GHz: (a)  $x$ - $y$  plane ( $\theta = 90$ ), (b)  $x$ - $z$  plane ( $\varphi = 0$ ), and  $y$ - $z$  plane ( $\varphi = 90$ ).

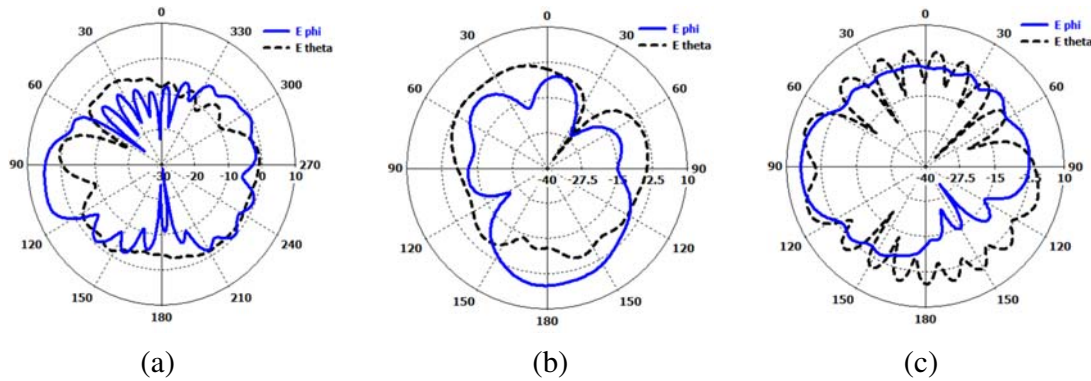


**Figure 11.** Radiation patterns of the proposed PIFA at 9.7 GHz: (a)  $x$ - $y$  plane ( $\theta = 90$ ), (b)  $x$ - $z$  plane ( $\varphi = 0$ ), and  $y$ - $z$  plane ( $\varphi = 90$ ).

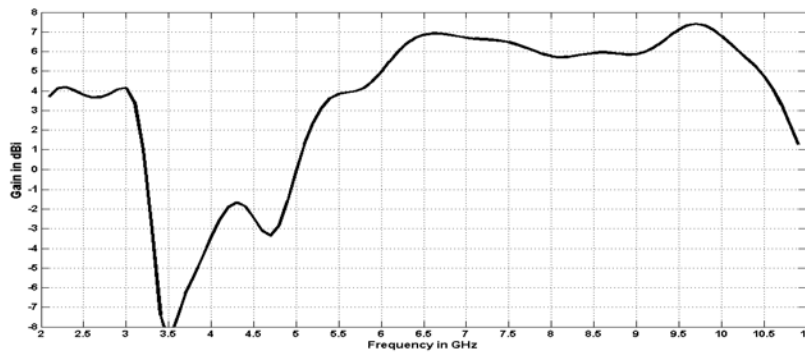


**Figure 12.** Gain of the proposed PIFA.

### 3.4. Specific Absorption Rate

With the increasing use of mobile phones, some researches have been carried out on electromagnetic interactions between the human body, in particular, the head and the antenna of the mobile phone and the risk of electromagnetic fields radiated by the handset on health [18,19]. SAR is a fundamental parameter in the risk analysis to the health of absorbing electromagnetic energy in the human body [20,21]. It assesses the amount of power absorbed per unit mass of tissue during the use of

mobile phone. This parameter can be calculated by the following equation:

$$SAR = \frac{\sigma |E|^2}{2\rho} \tag{2}$$

where  $\rho$  (kg/m<sup>3</sup>) and  $\sigma$  (S/m) are the body tissue density and conductivity, respectively.  $E$  (V/m) is the root-mean-square (rms) value of the electric field strength in the tissue. The SAR analysis was done by the CST microwave studio software. Specific Anthropomorphic Mannequin (SAM) is used as a phantom human head model to calculate SAR. To receive results close to reality, the parameters used for the model of the human head are shown in Table 3. Fig. 13 presents two PIFA positions at the top and bottom ground planes. The distance between the antenna and the human head is 2 mm. The reference power is set to 0.5 W. The results of simulated SAR are given in Fig. 14 (at 2.5 GHz) and Fig. 15 (at 5.2 GHz) in both standards on an average of 1 g tissue in Europe and on an average of 10 g tissue in USA.

**Table 3.** The parameters used for the human head model.

SAM Phantom Materiel	Relative permittivity ( $\epsilon_r$ )	Conductivity ( $\sigma(\frac{S}{m})$ )	Density ( $\rho(\frac{Kg}{m^3})$ )
SAM liquid	42	0.99	1000
SAM shell	5	0.0125173	0

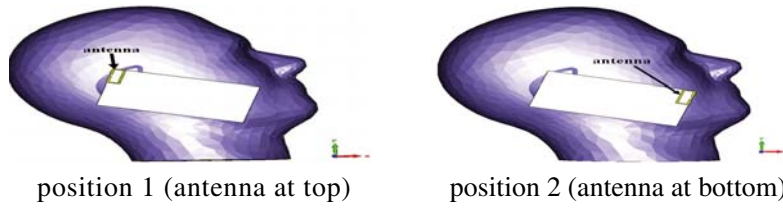


**Figure 13.** SAR simulation model and antenna positions: antenna at top, and antenna at bottom.

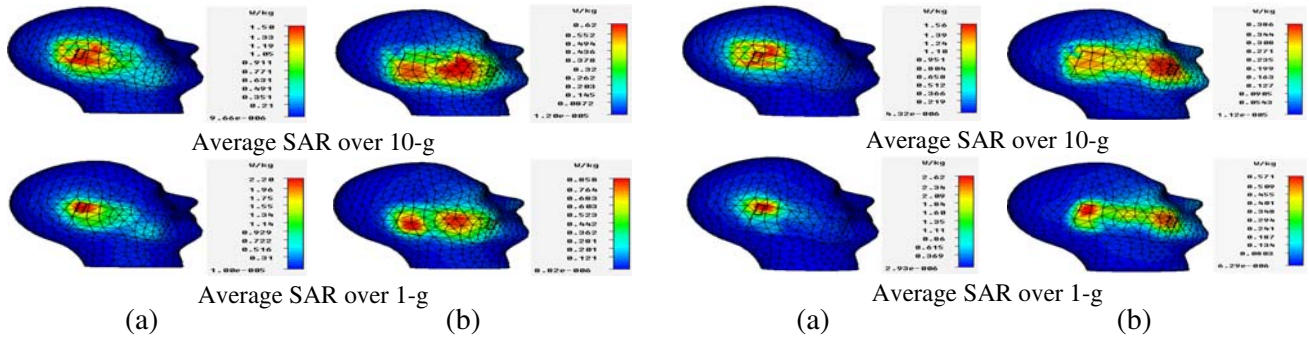


**Figure 14.** SAR distributions at 2.5 GHz for two antenna positions ((a) top position, and (b) bottom position).

**Figure 15.** SAR distributions at 5.2 GHz for two antenna positions ((a) top position, and (b) bottom position).

The obtained SAR results are shown in Table 4. From Table 4, we can see that the SAR values for the proposed antenna are below the limit specified by the two standards. By comparing the results in the two positions (1 and 2), we notice that position 2 is better than position 1 because the SAR results in position 2 are lower than their counterparts in position 1.

Figures 16(a) and 16(b) show the variation of SAR with the distance between the antenna and the human head at 2.5 GHz and 5.2 GHz, respectively. We notice from these figures that SAR values

**Table 4.** The maximum SAR values of the proposed PIFA at 2.5 GHz and 5.2 GHz.

Frequency	$SAR_{\max 10g}$ (position 1)	$SAR_{\max 1g}$ (position 1)	$SAR_{\max 10g}$ (position 2)	$SAR_{\max 1g}$ (position 2)
$f_r = 2.5$ GHz	$1.5(\frac{W}{Kg})$	$2.2(\frac{W}{Kg})$	$0.62(\frac{W}{Kg})$	$0.858(\frac{W}{Kg})$
$f_r = 5.2$ GHz	$1.56(\frac{W}{Kg})$	$2.62(\frac{W}{Kg})$	$0.386(\frac{W}{Kg})$	$0.571(\frac{W}{Kg})$

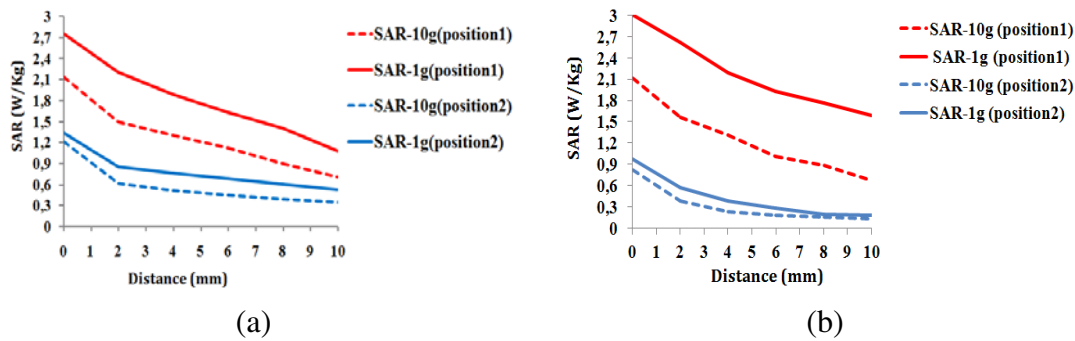


**Figure 16.** Variation of SAR in terms of the distance from the head: (a) at 2.5 GHz, and (b) at 5.2 GHz.

decrease by increasing the distance. This is simply because the RF power decreases with the increase in distance between the antenna and the human head, which agrees with [19–21].

#### 4. CONCLUSION

A new compact dual-band PIFA for mobile handsets has been proposed. The proposed antenna has been designed to operate in the WLAN (2.4, 5.2, and 5.8 GHz), Bluetooth (2.4 GHz), HiperLAN2 (5.2 and 5.6 GHz), LTE2500 (2.5 GHz) and WIMAX (5.5 GHz) bands. The integration of T-shaped slot in the radiating patch and the addition of two elements in the side of PIFA are two techniques that have been used to improve the bandwidth of the proposed antenna. Good radiation characteristics are at all resonant frequencies, with peak average gain around 4 dBi at 2.4 GHz and 7 dBi at 5.4 GHz. The results of the simulation and measurement for the proposed antenna show a good agreement in terms of  $S_{11}$ . Acceptable SAR values at different operating frequencies are achieved. SAR results indicate that by placing the proposed PIFA from the top position to the bottom position of the mobile phone, it is possible to get acceptable SAR values. The structure of the proposed antenna is easy to manufacture and modified for various mobile purposes.

#### ACKNOWLEDGMENT

The authors would like to express their sincere gratitude to the support by Naima A. Touhami of Electronics, Instrumentation and microwave Laboratory, Faculty of Sciences, Abdelmalek Essadi University, Tetouan, Morocco.

#### REFERENCES

- Hirose, H. and M. Miyake, “Gain improvement of a planar inverted F antenna on a handset by passive loading,” *Antennas and Propagation Society International Symposium*, Vol. 2, 1128–1131, 1995.
- Morishita, H., Y. Kim, and K. Fujimoto, “Design concept of antennas for small mobile terminals and the future perspective,” *IEEE Antennas Propag. Mag.*, Vol. 44, No. 5, 30–43, 2002.

3. Taga, T. and K. Tsunekawa, "Performance analysis of a built-in planar inverted-F antenna for 800 MHz band portable radio units," *IEEE J. Sel. Areas Commun.*, Vol. 5, No. 5, 921–929, 1987.
4. Hall, P. S., E. Lee, and C. T. P. Song, *Printed Antennas for Wireless Communications*, Chapter: Planar Inverted-F Antennas, John Wiley and Sons, Ltd, 2007.
5. Lin, D.-B., I.-T. Tang, and M.-Z. Hong, "A Compact quad-band pifa by tuning the defected ground structure for mobile phones," *Progress In Electromagnetics Research B*, Vol. 24, 173–189, 2010.
6. Gomez-Villanueva, R., R. Linares-y-Miranda, J. A. Tirado-Mendez, and H. Jardon-Aguilar, "Ultra-wideband planar inverted-F antenna (PIFA) for mobile phone frequencies and ultra-wideband applications," *Progress In Electromagnetics Research C*, Vol. 43, 109–120, 2013.
7. Chattha, H. T., Y. Huang, and Y. Lu, "PIFA bandwidth enhancement by changing the widths of feed and shorting plates," *IEEE Antennas Wirel. Propag. Lett.*, Vol. 8, 637–640, 2009.
8. Ibnyaich, S., A. Ghammaz, and M. M. Hassani, "Planar inverted-F antenna with J-shaped slot and parasitic element for ultra-wide band application," *Int. J. Microw. Wirel. Technol.*, Vol. 4, No. 06, 613–621, 2012.
9. Chattha, H. T., Y. Huang, Y. Lu, and X. Zhu, "Further bandwidth enhancement of PIFA by adding a parasitic element," *Antennas Propagation Conference, LAPC*, 213–216, Loughborough, 2009.
10. Gomez-Villanueva, R., R. Linares-y-Miranda, J. A. Tirado-Mendez, and H. Jardon-Aguilar, "Very broadband PIFA antenna for mobile communications and ultrawideband services," *Microw. Opt. Technol. Lett.*, Vol. 56, No. 2, 313–316, 2014.
11. Abedin, M. F. and M. Ali, "Modifying the ground plane and its effect on planar inverted-F antennas (PIFAs) for mobile phone handsets," *IEEE Antennas Wirel. Propag. Lett.*, Vol. 2, No. 1, 226–229, 2003.
12. Picher, C., J. Anguera, A. Cabedo, C. Puente, and S. Kahng, "Multiband handset antenna using slots on the ground plane: Considerations to facilitate the integration of the feeding transmission line," *Progress In Electromagnetics Research C*, Vol. 7, 95–109, 2009.
13. Man, M. Y., R. Yang, Z. Y. Lei, Y. J. Xie, and J. Fan, "Ultra-wideband planar inverted-F antennas with cut-etched ground plane," *Electron. Lett.*, Vol. 48, No. 14, 817–818, 2012.
14. Elsadek, H. and D. M. Nashaat, "Multiband and UWB V-shaped antenna configuration for wireless communications applications," *IEEE Antennas Wirel. Propag. Lett.*, Vol. 7, 89–91, 2008.
15. Saluja, N. and R. Khanna, "Design, analysis, and fabrication of a novel multiband folded edge compact size fractal PIFA for WiFi/LTE/WiMAX/WLAN application," *Microw. Opt. Technol. Lett.*, Vol. 56, No. 12, 2836–2841, 2014.
16. Janapsatya, J., K. P. Esselle, and T. S. Bird, "A dual-band and wideband planar inverted-F antenna for WLAN applications," *Microw. Opt. Technol. Lett.*, Vol. 50, No. 1 138–141, 2008.
17. Row, J. S., "Experimental studies of the dual-band planar inverted-F antenna with a U-shaped slot," *Microw. Opt. Technol. Lett.*, Vol. 37, No. 5, 359–336, 2003.
18. Han, Y.-N., Y.-H. Lu, N. Liu, and P.-F. He, "SAR distribution in visible human head exposure to the field radiated by crt computer monitors," *International Conference on Microwave and Millimeter Wave Technology, ICMMT'07*, 1–4, 2007.
19. Watanabe, S., M. Taki, T. Nojima, and O. Fujiwara, "Characteristics of the SAR distributions in a head exposed to electromagnetic fields radiated by a hand-held portable radio," *IEEE Trans. Microw. Theory Tech.*, Vol. 44, No. 10, 1874–1883, 1996.
20. Khodabakhshi, H. and A. Cheldavi, "Numerical analysis of human head interaction with PIFA antennas in cellular mobile communications," *Progress In Electromagnetics Research B*, Vol. 22, 359–377, 2010.
21. Montaser, A. M., K. R. Mahmoud, and A. H. Elmikati, "An interaction study between PIFAs handset antenna and a human hand-head in personal communications," *Progress In Electromagnetics Research B*, Vol. 37, 21–42, 2012.